crystals

MDPI

Article

Helimagnetism in $MnBi_2Se_4$ Driven by Spin-Frustrating Interactions Between Antiferromagnetic Chains

Judith K. Clark [1,†], Chongin Pak [1,2,†], Huibo Cao [3] and Michael Shatruk [1,2,*]

[1] Department of Chemistry and Biochemistry, Florida State University, Tallahassee, FL 32306, USA; jkr17e@my.fsu.edu (J.K.C.); cpak@asc.magnet.fsu.edu (C.P.)
[2] National High Field Magnetic Laboratory, Tallahassee, FL 32310, USA
[3] Neutron Scattering Division, Oak Ridge National Laboratory, Oak Ridge, TN 37830, USA; caoh@ornl.gov
* Correspondence: shatruk@chem.fsu.edu
† Both authors contributed equally to this work.

Abstract: We report the magnetic properties and magnetic structure determination for a linear-chain antiferromagnet, $MnBi_2Se_4$. The crystal structure of this material contains chains of edge-sharing $MnSe_6$ octahedra separated by Bi atoms. The magnetic behavior is dominated by intrachain antiferromagnetic (AFM) interactions, as demonstrated by the negative Weiss constant of −74 K obtained by the Curie–Weiss fit of the paramagnetic susceptibility measured along the easy-axis magnetization direction. The relative shift of adjacent chains by one-half of the chain period causes spin frustration due to interchain AFM coupling, which leads to AFM ordering at T_N = 15 K. Neutron diffraction studies reveal that the AFM ordered state exhibits an incommensurate helimagnetic structure with the propagation vector k = (0, 0.356, 0). The Mn moments are arranged perpendicular to the chain propagation direction (the crystallographic b axis), and the turn angle around the helix is 128°. The magnetic properties of $MnBi_2Se_4$ are discussed in comparison to other linear-chain antiferromagnets based on ternary mixed-metal halides and chalcogenides.

Keywords: magnetic structure; spin frustration; helimagnet; neutron diffraction

Citation: Clark, J.K.; Pak, C.; Cao, H.; Shatruk, M. Helimagnetism in $MnBi_2Se_4$ Driven by Spin-Frustrating Interactions Between Antiferromagnetic Chains. *Crystals* **2021**, *11*, 242. https://doi.org/10.3390/cryst11030242

Academic Editor: Andrei Vladimirovich Shevelkov

Received: 1 February 2021
Accepted: 24 February 2021
Published: 27 February 2021

1. Introduction

Frustrated magnetic interactions in crystalline materials result in exotic magnetic phenomena and complex spin textures in magnetically ordered states [1–4]. Low-dimensional magnetic systems feature hierarchical exchange interactions that, in the case of magnetic ordering, can lead to the ground state magnetic structure being defined by a combination of competing exchange coupling pathways rather than by the dominant nearest-neighbor interactions [5,6]. A simple example of such behavior can be demonstrated by considering two parallel chains of magnetic moments, with the intrachain exchange coupling (J_1) being stronger than the interchain one (J_2). In the case of antiferromagnetic (AFM) exchange, the chains with the exact match in the relative location of their moments form spin ladders (Figure 1a) that experience no conflict in setting into an AFM ordered state. If the chains, however, are displaced by half a period in the chain direction (Figure 1b), the weaker exchange interactions defined by J_2 conflict with the stronger interactions defined by J_1, causing spin frustration. The ratio between these exchange constants and the local magnetic anisotropy of the interacting spins will dictate the spin texture attained by the material upon magnetic ordering. The strongest frustration takes place when $J_1 = J_2$. But even in the case of well-defined chains, when J_1 dominates, the transverse action of the J_2 parameter might lead to the deviation from collinear magnetic ordering along the chain and the formation of helical magnetic structures.

An ideal one-dimensional (1D) magnet should not exhibit long-range ordering at a finite temperature. Hence, the magnetic ordering in any chain compound depends on the J_2/J_1 ratio—the smaller this ratio, the lower the AFM ordering temperature (T_N) relative

to the value that could be hypothetically expected from the strength of the intrachain exchange coupling. A well-studied example of an AFM Heisenberg chain is $(Me_4N)[MnCl_3]$ (Me = methyl). The large interchain separation of 9.15 Å between the $S = 5/2$ Mn^{2+} ions, as compared to the much shorter intrachain distance of 3.25 Å, effectively isolates the chains of the Mn spins. As a result, the experimental $T_N = 0.84$ K is substantially smaller than the temperature of 76 K calculated from the molecular field theory based on the intrachain exchange value of $J_1 = -6.3$ K (estimated from high-temperature magnetic susceptibility measurements) [7]. The strong quasi-1D nature of magnetic coupling in $(Me_4N)[MnCl_3]$ allowed observation of temperature-dependent soliton excitations both above and below T_N, making it a unique 1D magnetic system [8].

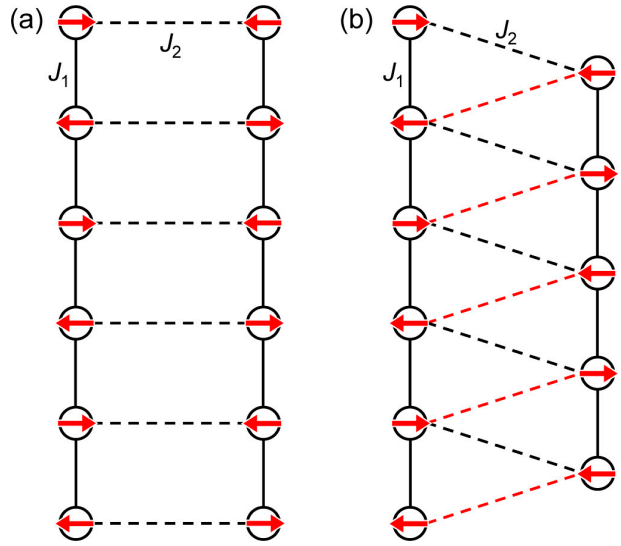

Figure 1. Two chains of magnetic moments with antiferromagnetic (AFM) exchange coupling both within (J_1) and between (J_2) the chains. While all pairwise AFM interactions can be satisfied in the ar-rangement (**a**), spin frustration develops in the arrangement (**b**) due to the half-period shift between the chains. This shift results in the orientation of spins that conflicts with the AFM ex-change constant J_1 (the conflicting interactions are highlighted in red).

As the distance between the chains decreases, the J_2 exchange pathway begins to play a more notable role. Thus, $(MeNH_3)[MnCl_3(H_2O)_2]$ and $Cs[MnCl_3(H_2O)_2]$ exhibit AFM ordering at 4.1 K [9] and 4.9 K [10], respectively. In K_2MnS_2 and K_2MnSe_2, with even closer arranged chains, the T_N value increases to 17 K, and the J_1 value was estimated to be above –14 K [11]. The spin frustration observed in these two structures leads to a helical magnetic structure, with the moments being perpendicular to the chain propagation direction.

Helimagnetic ordering can be expected in other quasi-1D systems with the relative spin arrangement of Figure 1b. Spin frustration afforded by such a configuration can lead to incommensurate magnetic structures, resulting in two-dimensional vortex domain walls that are not typically seen in bulk magnetic systems [12]. Such vortex domain walls are sensitive to external currents, thus creating prospects for leveraging magnetoelectric coupling in helimagnets for applications in low-power devices and rapid-access memory.

Many mixed-metal ternary halides and chalcogenides feature chain-like structural motifs of the magnetic transition metal ions. For many of these compounds, however, the magnetic structures remain unknown. The interesting fundamental properties of chain magnets, such as the observation of soliton excitations and helimagnetism [13], and their practical appeal for future technologies that leverage magnetoelectric coupling [14] call for further investigation of 1D magnetic systems. In this vein, our attention was grabbed by $MnBi_2Se_4$, a chain antiferromagnet with $T_N = 15$ K. The original report on the magnetic properties of this material proposed a collinear AFM structure, with a possibility of weak spin canting [15]. We notice, however, that the spin configuration in this material

corresponds to the one shown in Figure 1b, and, thus, some degree of spin frustration should be expected. Herein, we report a more detailed study of magnetic properties of $MnBi_2Se_4$ by single-crystal magnetic measurements and the determination of its magnetic structure by single-crystal neutron diffraction. We show that this material, indeed, exhibits an incommensurate magnetic structure with helical spin arrangement.

2. Materials and Methods

2.1. Crystal Growth

Single crystals were obtained following the chemical vapor transport (CVT) method described earlier [16]. Powders of Mn (Alfa Aesar, 99.98%), Bi (VWR, 99.999%), and Se (VWR, 99.999%) were combined in a stoichiometric ratio in an Ar-filled dry box (content of O_2 < 0.5 ppm). The sample was sealed in a fused silica tube evacuated to the pressure of ~10^{-4} Torr. The sample was heated to 580 °C and held at that temperature for 7 days. The obtained product was ground to a fine powder. The binary MnSe, required for crystal growth experiments, was synthesized by a stoichiometric reaction between Mn and Se sealed in an evacuated silica tube and heated at 600 °C for 4 days. The obtained powders of $MnBi_2Se_4$ and MnSe were combined in an 85:15 ratio (the total mass ~300 mg), with 3–4 mg of I_2 added as a transport agent, and sealed in a 14 mm inner diameter silica tube under vacuum (~10^{-4} Torr). The length of the sealed tube was 305 mm. The tube was placed horizontally in a two-zone furnace, with the source and sink sides set to 700 °C and 600 °C, respectively, and maintained at this temperature gradient for 7 days, after which it was quenched into water. Large black needle-like single crystals of $MnBi_2Se_4$ were collected from the sink zone of the tube.

2.2. Powder X-ray Diffraction (PXRD)

PXRD was used to characterize bulk precursors used for the crystal growth. The measurements were carried out at room temperature using a Panalytical X'Pert Pro diffractometer (Malvern Panalytical, Malvern, UK) with an X'Celerator detector and Cu-Kα radiation (λ = 1.54187 Å). Each pattern was recorded in the 2θ range from 10° to 80° with a step of 0.05° and the total collection time of 1 h. The data analysis was performed with HighScore Plus [17].

2.3. Single-Crystal X-ray Diffraction (SCXRD)

SCXRD was carried out at room temperature on a Rigaku-Oxford Diffraction Synergy-S diffractometer equipped with a HyPix detector and a monochromated Mo-*K*α radiation source (λ = 0.71073 Å). The unit cell was determined from ~50 diffraction frames using the CrysAlis software package [18].

2.4. Magnetic Measurements

Magnetic measurements were performed on a single-crystal sample using a Quantum Design SQUID magnetometer MPMS-XL. DC magnetic susceptibility was measured in the temperature range of 1.8–300 K under applied magnetic field of 5 kOe, with the crystal being aligned parallel or perpendicular to the applied field.

2.5. Single Crystal Neutron Diffraction

Single crystal neutron diffraction experiments were performed at the High Flux Isotope Reactor at Oak Ridge National Laboratory (ORNL) using the HB-3A four-circle diffractometer [19]. Neutrons with wavelength of λ = 1.005 Å were selected by a bent silicon monochromator Si-331. The data were collected at 4 and 300 K. Intensity of a selected magnetic peak was also measured as a function of temperature to determine the magnetic ordering temperature. Refinement of the nuclear structure and magnetic structure determination were carried out using the FULLPROF software [20].

3. Results

3.1. Crystal Growth

Crystals of $MnBi_2Se_4$ were obtained by the previously reported CVT method [16]. The source material was a mixture of pre-synthesized $MnBi_2Se_4$ and MnSe powders (Figure S1, see supplementary materials), and a small amount of I_2 served as a transport agent. While a small quantity of Bi_2Se_3 can be seen in the PXRD pattern of $MnBi_2Se_4$, we found that this minor byproduct did not have any adverse effect on the quality of CVT-grown crystals of $MnBi_2Se_4$. The CVT in the 700 °C → 600 °C temperature gradient resulted in the growth of long black needle-like crystals with metallic luster (Figure 2a) in the colder zone of the tube. SCXRD analysis revealed unit cell parameters within 2% of the previously reported unit cell parameters of the monoclinic $MnBi_2Se_4$ phase (space group $C2/m$, a = 13.55(5) Å, b = 4.102(4) Å, c = 15.38(5) Å, β = 115.7(1)° in this work, compared to a = 13.384(3) Å, b = 4.0925(8) Å, c = 15.224(3) Å, β = 115.6(1)° in [15]). The minor difference might be caused by a slight antisite disorder in the occupancy of the Mn and Bi sites, as has been reported before [16]. In the crystal structure of this compound, $MnSe_6$ octahedra share edges to form infinite chains parallel to the b axis of the lattice. The chains are separated by Bi atoms. The intrachain Mn–Mn distance is 4.070 Å, while the interchain Mn–Mn distance is 6.964 Å, and the neighbor chains are shifted relative to each other by one-half of the b translation (Figure 2b).

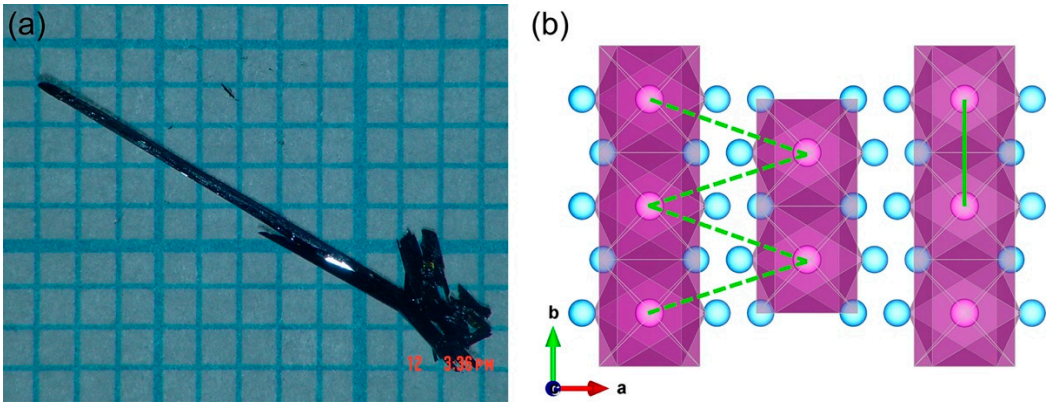

Figure 2. (**a**) A single crystal of $MnBi_2Se_4$ grown by the chemical vapor transport (CVT) technique. The scale of the background paper is 1 mm. (**b**) The nearest intrachain (solid line) and interchain (dashed lines) Mn–Mn contacts in the crystal structure of $MnBi_2Se_4$, corresponding to the J_1 and J_2 magnetic exchange constants, respectively.

3.2. Magnetic Properties

Previous magnetic measurements on powder samples of $MnBi_2Se_4$ revealed long-range AFM ordering at T_N = 15 K [15,16]. To establish the direction of magnetic anisotropy, we performed magnetic measurements of an oriented single-crystal of $MnBi_2Se_4$. The magnetic susceptibility (χ) measurements with the magnetic field applied perpendicular to the b axis ($H_\perp$) confirmed the AFM ordering at T_N = 15 K (Figure 3a). On the other hand, there was no obvious anomaly in the magnetization curve measured with the field parallel to the b axis ($H_\parallel$). These observations are consistent with the hypothesis that the Mn moments undergo AFM ordering with the preferred orientation perpendicular to the chain propagation direction. The field-dependent magnetization isotherms measured at 1.8 K (Figure 3b) showed lower values when measured under $H_\perp$, which agrees with the expectation of the more efficient cancellation of spins along the easy magnetization direction in an antiferromagnet.

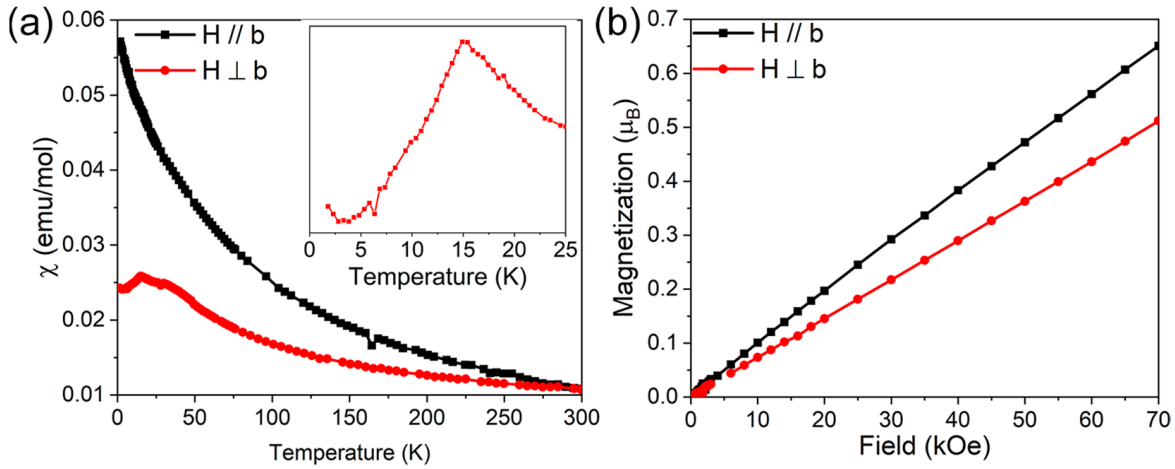

Figure 3. Temperature dependence of field-cooled (FC) magnetic susceptibility at 5 kOe (**a**) and field dependence of magnetization at 1.8 K (**b**) measured on a single crystal of $BiMn_2Se_4$ with the magnetic field applied perpendicular and parallel to the long axis (the crystallographic *b* axis).

The temperature dependence of parallel inverse susceptibility ($1/\chi_{\parallel}$) above 150 K was fit to the Curie–Weiss law, $1/\chi_{\parallel} = (C - \theta)/T$, but a modified Curie–Weiss law, $1/\chi_{\perp} = (C - \theta)/T + \chi_0$, where χ_0 is a temperature-independent paramagnetic term, was needed to obtain a meaningful fit for $\chi_{\perp}$ (Figure S2). The best-fit values obtained were $C_{\perp}$ = 3.2(3) emu·K/mol and $C_{\parallel}$ = 3.74(4) emu·K/mol for the Curie constants and $\theta_{\perp} = -74(13)$ K and $\theta_{\parallel} = -44(3)$ K for the Weiss constants, with χ_0 = 0.0216(6) emu/mol. The need to use the modified Curie–Weiss law to fit the temperature dependence of $1/\chi_{\perp}$ is likely a manifestation of the system being substantially far from the purely paramagnetic behavior, as a result of the strong intrachain AFM correlations acting in the studied temperature range. This shortcoming is a likely source of the large error in the determination of $\theta_{\perp}$.

The values of the effective magnetic moment, calculated from the Curie constants, are $(\mu_{eff})_{\perp}$ = 5.13 μ_B and $(\mu_{eff})_{\parallel}$ = 5.48 μ_B. These values are slightly lower than the expectation value of 5.92 μ_B for the high-spin Mn^{2+} ion (S = 5/2). The slightly lower value of μ_{eff} and the more negative value of θ observed for the measurements under $H_{\perp}$, as compared to those under $H_{\parallel}$, are consistent with the preferred orientation of AFM-coupled Mn moments perpendicular to the chain direction. Field-dependent magnetization measurements at 1.8 K revealed a linear increase in magnetization (M) with the maximum values $M_{\perp}$ = 0.51 μ_B and $M_{\parallel}$ = 0.65 μ_B at 7 T (Figure 3b). Such behavior is also in agreement with the AFM ordered magnetic moments being aligned perpendicular to the *b* axis.

3.3. Magnetic Structure

The magnetic structure was determined by single-crystal neutron diffraction performed on the HB-3A diffractometer at ORNL. The nuclear structure was refined based on the data collected at 300 K, after which the temperature was lowered to 4.2 K to search for magnetic peaks. The new peaks that appeared due to long-range AFM ordering were successfully indexed with the propagation vector k = (0, 0.356, 0), indicating an incommensurate magnetic structure, with the Mn moments forming a helical arrangement perpendicular to the chain propagation direction (Figure 4a). The incremental turn angle for the rotation of Mn moments around the chain axis can be calculated from the relationship $\alpha = 2\pi k$, which yields the angle of 128° between the ordered magnetic moments on the adjacent Mn sites (Figure 4b). The summary of the magnetic structure refinement parameters is provided in Table 1. The refined magnetic moment was 3.45(14) μ_B per Mn site, which is comparable to the majority of values of magnetic moments determined for the related ternary manganese chalcogenide and halide AFM materials summarized in Table 2 (see the Discussion section below).

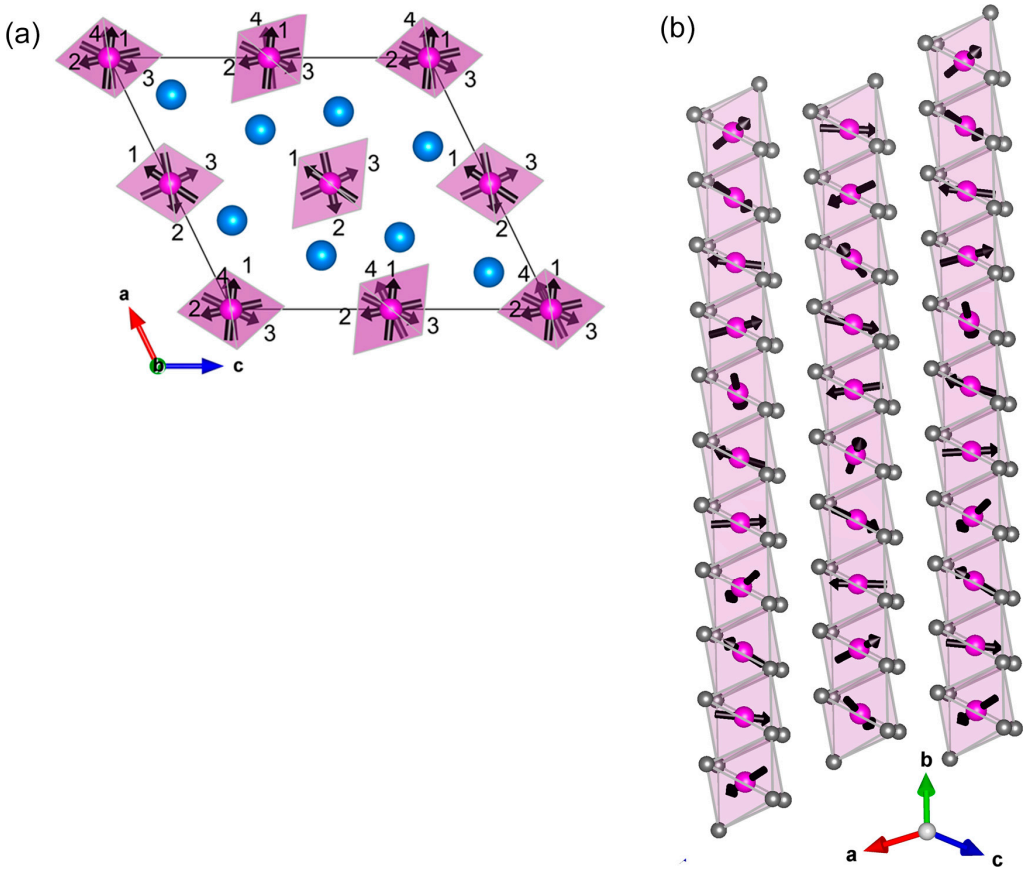

Figure 4. (**a**) A view of the magnetic structure of $MnBi_2Se_4$ down the *b* axis, emphasizing the rotation angle of 128° between the adjacent magnetic moments. The numbers refer to the sequence of moments rotating around the *b* axis. (**b**) A side view of chains of helically ordered magnetic moments.

Table 1. Details of the magnetic structure refinement parameters for $MnBi_2Se_4$.

Temperature, K	4.2
Wavelength, Å	1.005
Magnetic space group	$\overline{C}1$
Unit cell parameters	
a, Å	13.357
b, Å	4.073
c, Å	15.301
β, Å	115.89
Propagation vector, *k*	0, 0.356, 0
Magn. moment, *m*(Mn), μ_B	3.45(14)
R_F	0.0604
χ^2	1.46

To follow the order parameter, the intensity of the magnetic peak (0, 0.356, 2) was measured as a function of temperature, in the cooling mode from 25 to 4.2 K. The dependence shown in Figure S3 clearly confirms the AFM ordering, as the magnetic peak rapidly increases in intensity at 13 K, which is only slightly lower than the value of T_N = 15 K determined by magnetic measurements. The slight difference in the ordering temperatures might be caused by the influence of the external magnetic field that was applied to the sample during the magnetic susceptibility measurements, while the neutron diffraction

experiment was carried out in zero applied field. Although applied magnetic field typically leads to a decrease in the T_N values of a regular (collinear) antiferromagnet, its influence on a spin-frustrated system can be opposite. Indeed, as the applied field tends to suppress the spin-frustrating interactions, one could hypothesize that such a suppression might lead to the increase in T_N as observed in the present case.

4. Discussion

It is of interest to compare the magnetic properties and crystal and magnetic structures of $MnBi_2Se_4$ and related ternary chalcogenides and halides with chain-like arrangement of Mn magnetic moments. (We limit this comparison to the Mn-containing compounds to avoid the addition of other factors, such as the single-ion spin value and magnetic anisotropy, which also influence the values of magnetic parameters and adopted magnetic structure.) Based on the considerations outlined in the introduction to this paper, we classify the relative arrangement of the chains as either "zigzag", implying that the adjacent chains are shifted relative to one another by 1/2 of the chain repeat distance (Figure 1b), or "ladder", implying that they are not shifted (Figure 1a). The crystal structures of $RbMnBr_3$ [21], $CsMnBr_3$ [22], and $CsMnI_3$ [23] exhibit the ladder arrangement of two nearest chains. The magnetic moment per Mn site and the ratio of the intrachain to interchain Mn–Mn distances are similar for all three compounds. Nevertheless, the hexagonal symmetry of the lattice imposes the regular triangular pattern of chains (when viewed down the chain propagation direction), which unavoidably leads to the geometrical frustration of the interchain magnetic interactions described by the J_2 constant. As a result, these compounds form helimagnetic structures (Table 2).

Table 2. Properties and Magnetic-Chain Halides and Chalcogenides.

Compound	T_N (K)	θ (K)	μ (μ_B)	μ_{eff} (μ_B)	Intrachain Distance (Å)	Interchain Distance (Å)	Intra/Inter Ratio	Interchain Pattern	Turn Angle
$RbMnBr_3$ [24]	8.8	–	3.6	–	3.271	7.462	0.4383	Ladder	130°
$CsMnBr_3$ [25]	8.45	–167	3.5	6.4	3.259	7.618	0.4278	Ladder	120°
$CsMnI_3$ [26]	11.1	–	3.7	–	3.479	8.196	0.4244	Ladder	50°
K_2MnSe_2 [11]	17	–	2.27	–	3.220	7.507	0.4289	Ladder	208°
$MnSb_2S_4$ [27]	25	–63	4.6	6.02	3.799	6.651	0.5711	Zigzag	132°
$MnSb_2Se_4$ [28]	20	–74	–	5.82	3.965	6.832	0.5803	Zigzag	–
$MnBi_2Se_4$	15	–74	3.3	5.13	4.070	6.964	0.5844	Zigzag	128°

A similar situation is observed in the structure of $K_2MnS_{2-x}Se_x$ ($0 \leq x \leq 2$), where the nearest chains are not shifted with respect to each other along the chain propagation direction, but the overall crystal packing results in a triangulated pattern of chains, thus causing magnetic frustration and helimagnetic structure for the entire series of solid solutions [11]. Interestingly, the propagation vector and, thus, the turn angle of the spin helix, remain the same, irrespective of the S/Se ratio in the sample.

Similar to $MnBi_2Se_4$, the isostructural compound $MnSb_2S_4$ undergoes AFM ordering at T_N = 25 K and exhibits an incommensurate helimagnetic structure with α = 132° [27], which can be viewed as emerging from the spin frustration caused by the relative shift of the adjacent chains by one-half of the chain repeat distance (Figure 2b). Besides, when these structures are viewed down the chain propagation direction, the triangular arrangement of chains becomes evident (Figure 4a), despite the slight distortion that lowers the symmetry to the monoclinic space group $C2/m$. This triangulated arrangement of interchain contacts described by the J_2 exchange constant should also contribute to spin frustration. We expect that the same helimagnetic structure should be observed for the isostructural compound $MnSb_2Se_4$ that orders AFM at T_N = 20 K [28]. These three materials, which belong to the $FeSb_2Se_4$ structure type, exhibit gradual decrease in the T_N value from $MnSb_2S_4$ to $MnSb_2Se_4$ to $MnBi_2Se_4$. This trend can be explained by the increasing radii of the post-transition metal and chalcogen atoms, which lead to the larger interchain separation and smaller J_2 values (Table 2).

It would be of interest to explore these and related materials by inelastic neutron scattering to allow the direct measurement of the J_1 and J_2 exchange coupling constants. Furthermore, helimagnetic structures are of current interest in the search for new multiferroic materials [14], and $MnSb_2Se_4$ was theoretically predicted to be a good candidate for multiferroic behavior [29]. Studies in these directions are currently underway in our laboratory, and their results will be reported in due course.

Supplementary Materials: The following are available online at https://www.mdpi.com/2073-4352/11/3/242/s1, Additional powder diffraction patterns, Curie–Weiss fits of inverse magnetic susceptibility, and temperature dependence of the magnetic peak intensity from neutron diffraction measurements.

Author Contributions: Conceptualization, M.S. and C.P.; methodology, C.P. and J.K.C.; software, J.K.C., C.P., and H.C.; validation, H.C., J.K.C., and C.P.; formal analysis, H.C., J.K.C., and C.P.; investigation, H.C., J.K.C., and C.P.; resources, M.S.; data curation, H.C., J.K.C., and C.P.; writing—original draft preparation, J.K.C. and M.S.; writing—review and editing, C.P. and H.C.; visualization, J.K.C.; supervision, M.S. and H.C.; project administration, M.S.; funding acquisition, M.S. All authors have read and agreed to the published version of the manuscript.

Funding: This research was supported by the National Science Foundation (DMR-1905499). The Rigaku Synergy-S single-crystal X-ray diffractometer used for crystallographic work was acquired through the NSF MRI program (award CHE-1828362). J.K.C. acknowledges the support from the DOE Office of Science Graduate Student Research (SCGSR) Fellowship.

Institutional Review Board Statement: Not applicable.

Informed Consent Statement: Not applicable.

Data Availability Statement: All data pertinent to this work can be obtained upon request by contacting the corresponding author of the article.

Acknowledgments: The neutron diffraction experiments used resources at the High Flux Isotope Reactor, U.S. Department of Energy (DOE) Office of Science User Facility operated by the Oak Ridge National Laboratory. This research also used resources provided by the X-ray Crystallography Center (FSU075000XRAY) and the Materials Characterization Laboratory (FSU075000MAC) at the FSU Department of Chemistry and Biochemistry.

Conflicts of Interest: The authors declare no conflict of interest. The funders had no role in the design of the study; in the collection, analyses, or interpretation of data; in the writing of the manuscript; or in the decision to publish the results.

References

1. Ramirez, A.P. Strongly geometrically frustrated magnets. *Annu. Rev. Mater. Sci.* **1994**, *24*, 453–480. [CrossRef]
2. Lacroix, C. Frustrated metallic systems: A review of some peculiar behavior. *J. Phys. Soc. Jpn.* **2010**, *79*, 011008. [CrossRef]
3. Greedan, J.E. Geometrically frustrated magnetic materials. *J. Mater. Chem.* **2001**, *11*, 37–53. [CrossRef]
4. Kanazawa, N.; Seki, S.; Tokura, Y. Noncentrosymmetric magnets hosting magnetic skyrmions. *Adv. Mater.* **2017**, *29*, 1603227. [CrossRef] [PubMed]
5. Mikeska, H.-J.; Kolezhuk, A.K. One-dimensional magnetism. *Lect. Notes Phys.* **2004**, *645*, 1–83.
6. Richter, J.; Schulenburg, J.; Honecker, A. Quantum magnetism in two dimensions: From semi-classical Néel order to magnetic disorder. *Lect. Notes Phys.* **2004**, *645*, 85–153.
7. Dingle, R.; Lines, M.E.; Holt, S.L. Linear-chain antiferromagnetism in $[(CH_3)_4N][MnCl_3]$. *Phys. Rev.* **1969**, *187*, 643–648. [CrossRef]
8. Holyst, J.A.; Benner, H. Internal oscillations of solitons in $(CH_3)_4NMnCl_3$ above and below T_N. *Phys. Rev. B* **1995**, *52*, 6424–6430. [CrossRef] [PubMed]
9. Simizu, S.; Chen, J.Y.; Friedberg, S.A. Quasi-one-dimensional antiferromagnetism in $(CH_3NH_3)MnCl_3{\cdot}2H_2O$. *J. Appl. Phys.* **1984**, *55*, 2398–2400. [CrossRef]
10. Butterworth, G.J.; Woollam, J.A. Magnetic phase diagram of $CsMnCl_3{\cdot}2H_2O$. *Phys. Lett. A* **1969**, *29*, 259–260. [CrossRef]
11. Bhutani, A.; Behera, P.; McAuliffe, R.D.; Cao, H.; Huq, A.; Kirkham, M.J.; dela Cruz, C.R.; Woods, T.; Shoemaker, D.P. Incommensurate magnetism in $K_2MnS_{2-x}Se_x$ and prospects for tunable frustration in a triangular lattice of pseudo-1D spin chains. *Phys. Rev. Mater.* **2019**, *3*, 064404. [CrossRef]
12. Li, F.; Nattermann, T.; Pokrovsky, V.L. Vortex domain walls in helical magnets. *Phys. Rev. Lett.* **2012**, *108*, 107203. [CrossRef] [PubMed]

13. Vasiliev, A.; Volkova, O.; Zvereva, E.; Markina, M. Milestones of low-D quantum magnetism. *NPJ Quant. Mater.* **2018**, *3*, 18. [CrossRef]
14. Tokura, Y.; Seki, S. Multiferroics with spiral spin orders. *Adv. Mater.* **2010**, *22*, 1554–1565. [CrossRef]
15. Ranmohotti, K.G.S.; Djieutedjeu, H.; Poudeu, P.F.P. Chemical manipulation of magnetic ordering in $Mn_{1-x}Sn_xBi_2Se_4$ solid–solutions. *J. Am. Chem. Soc.* **2012**, *134*, 14033–14042. [CrossRef]
16. Nowka, C.; Gellesch, M.; Enrique Hamann Borrero, J.; Partzsch, S.; Wuttke, C.; Steckel, F.; Hess, C.; Wolter, A.U.B.; Teresa Corredor Bohorquez, L.; Büchner, B.; et al. Chemical vapor transport and characterization of $MnBi_2Se_4$. *J. Cryst. Growth* **2017**, *459*, 81–86. [CrossRef]
17. PANalytical B. *X'Pert HighScore Plus software v. 2.2b*; PANalytical B.V.: Almelo, The Netherlands, 2006.
18. PRO CrysAlis. *CrysAlis*; Oxford Diffraction Ltd.: Abingdon, UK, 2006.
19. Chakoumakos, B.C.; Cao, H.; Ye, F.; Stoica, A.D.; Popovici, M.; Sundaram, M.; Zhou, W.; Hicks, J.S.; Lynn, G.W.; Riedel, R.A. Four-circle single-crystal neutron diffractometer at the High Flux Isotope Reactor. *J. Appl. Crystallogr.* **2011**, *44*, 655–658. [CrossRef]
20. Rodríguez-Carvajal, J. Recent advances in magnetic-structure determination by neutron powder diffraction. *Phys. B* **1993**, *192*, 55–69. [CrossRef]
21. Goodyear, J.; Ali, E.M.; Sutherland, H.H. Rubidium tribromomanganate. *Acta Crystallogr. Sect. B* **1980**, *36*, 671–672. [CrossRef]
22. Goodyear, J.; Kennedy, D.J. The crystal structure of $CsMnBr_3$. *Acta Crystallogr. Sect. B* **1972**, *28*, 1640–1641. [CrossRef]
23. Seifert, H.J.; Kischka, K.H. Investigations on systems AX/MnX_2 (A = Li-Cs. TI: X = Cl, Br, I) by DTA and X-ray analysis. *Thermochim. Acta* **1978**, *27*, 85–93. [CrossRef]
24. Glinka, C.J.; Minkiewicz, V.J.; Cox, D.E.; Khattak, C.P. The magnetic structure of $RbMnBr_3$. *AIP Conf. Proc.* **1973**, *10*, 659–663.
25. Eibschütz, M.; Sherwood, R.C.; Hsu, F.S.L.; Cox, C.E. Magnetic ordering of the linear chain antiferromagnet $CsMnBr_3$. *AIP Conf. Proc.* **1973**, *10*, 684–688.
26. Zandbergen, H.W. Neutron powder diffraction and magnetic measurements on $CsMnI_3$. *J. Solid State Chem.* **1980**, *35*, 367–375. [CrossRef]
27. Léone, P.; Doussier-Brochard, C.; André, G.; Moëlo, Y. Magnetic properties and neutron diffraction study of two manganese sulfosalts: Monoclinic $MnSb_2S_4$ and benavidesite ($MnPb_4Sb_6S_{14}$). *Phys. Chem. Miner.* **2008**, *35*, 201–206. [CrossRef]
28. Djieutedjeu, H.; Makongo, J.P.A.; Rotaru, A.; Palasyuk, A.; Takas, N.J.; Zhou, X.; Ranmohotti, K.G.S.; Spinu, L.; Uher, C.; Poudeu, P.F.P. Crystal structure, charge transport, and magnetic properties of $MnSb_2Se_4$. *Eur. J. Inorg. Chem.* **2011**, *2011*, 3969–3977. [CrossRef]
29. Tian, C.; Lee, C.; Kan, E.; Wu, F.; Whangbo, M.-H. Analysis of the magnetic structure and ferroelectric polarization of monoclinic $MnSb_2S_4$ by density functional theory calculations. *Inorg. Chem.* **2010**, *49*, 10956–10959. [CrossRef] [PubMed]